Measurement 139 (2019) 134–139

Contents lists available at ScienceDirect

Measurement

journal homepage: www.elsevier.com/locate/measurement

Elasto – Plastic materials behavior evaluation according to different models applied in indentation hardness tests

A.L.M. Vargas, E. Blando, R. Hübler *

LMN – Laboratório de Materiais e Nanosciências, Sala 103, Prédio 96A, TECNOPUC, Escola de Ciências, PUCRS, Brazil

ARTICLE INFO

Article history:
Received 16 January 2017
Received in revised form 27 December 2018
Accepted 29 January 2019
Available online 1 March 2019

Keywords:
Instrumented hardness test
Nanoindentation
Hardness models

ABSTRACT

Instrumented Hardness Tests (IHT), also known as nanoindentation, establishes itself throughout the years as a standard method to characterize superficial elasto – plastic properties of materials, with a greater capability to evaluate thin films. The main advantage of this test lies on the application of dynamical load – unload cycles, generally with values of few mN and displacements below 200 nm, granting more information about the material beyond hardness, as elastic modulus, creep, fracture resistance, among others. However, the difficulty to achieve an adequate contact between sample and penetrator complicate the interpretation of its results. Several theoretical models were developed in order to diminish this effect achieving relative success. Each theory takes in consideration different aspects of the phenomenon and its application produces diverse mechanical properties values, which makes difficult the comparison among them. The aim of this work is to measure materials mechanical properties in accordance with ISO 14577 Martens model, the Oliver – Pharr (OP) method and the approximation developed by Gong, Miao and Peng (GMP) which are typically used on IHT, in order to find a possible relation among them. Aluminum, silicon (1 0 0) and soda-lime glass bulk materials were measured using a Fischerscope HV100 equipment with a Berkovich indenter. Dynamical load – unload cycles were applied to the samples with its maximum value ranging between 3 mN and 25 mN, during a total time of 120 s each cycle. The hardness calculation was performed according to the ISO 14577 Martens hardness model with indenter tip correction and considering the indentation size effect (ISE). The Oliver – Pharr method was calculated contemplating the non-linearity of the unload curve, adjusted by a power law. The Gong – Miao – Peng approximation was very similar to the OP technique, differing by the use of a virtual contact load and an indenter response based on a conical geometry instead the revolution paraboloid one, which is typically used. The results obtained confirm the hardness values variations among the models, which differ mostly at low load cycles. The comparison between the hardness calculations made by each model and the indenter response are presented as final result.

1. Introduction

The area of mechanical properties of materials, e.g., hardness and elastic moduli, is of major importance given the significant rise in the number of applications of these properties in diverse areas such as: Health science [1–7]; metal-mechanical industry [7–10]; elastomers [11]; military technology [12–13]; and oil and gas prospection [14–15]. Materials surface and thin films mechanical properties evaluation was very difficult in the past, mostly due to the lack of suitable techniques. On the early 90′s, the first computer controlled equipment capable of instantaneously measure the displacement and hardness using an indenter penetration were developed [16–18], permitting to apply and to monitor dynamically as much the penetration depth as the load used. This advance resulted in the directly hardness measurement, without the optical evaluation of the indenter impression, providing more data towards the material, as elastic modulus, creep, fracture strength, among others [19–23]. Nowadays, these equipment's can produce nanometric displacements (depth < 200 nm) with very low loads and were standardized by ISO 14577 [24] as IHT technique.

However, the low loads and displacements values achieved during test and the complexity to produce indenters with a perfect geometry generates contact problems between sample and indenter, which makes the results interpretation more intricate. These contact problems were related to several phenomena as pile-up, sink-in and residual contact stress. Innumerous models were developed through the years in order to evaluate satisfactorily

* Corresponding author.
E-mail address: hubler@pucrs.br (R. Hübler).

https://doi.org/10.1016/j.measurement.2019.01.090
0263-2241/

the elasto-plastic cycles and calculate the "real" hardness of materials. Among them, could be highlighted the Doerner – Nix approach [16–18], which is the first model to suppose the unload curve as linear, permitting the calculus of the hardness based on the contact stiffness between the material and the indenter, and the Oliver – Pharr model (OP) [25].

The main difference between the OP model and earlier models was the suggestion of non-linear unload curve, considering a power law fit as the best way to describe it. The approach uses the elastic contact theory developed by Sneddon for rigid penetrators with diverse geometries [26]. According to Sneddon, material hardness could be obtained with the determination of the contact stiffness S, which is described as:

$$S = \frac{2}{\sqrt{\pi}} E_r \sqrt{A} \tag{1}$$

where Er is the reduced elastic modulus and A is the projected contact area. Nevertheless, the S determination should be made through a function which describes satisfactorily the initial portion of the unload curve. According to the OP approach [25,27] this curve is well represented by a power function, obeying the equation:

$$P = \beta \, (h - h_f)^m \tag{2}$$

where $ß$ and m were empirically achieved by numerical adjustment parameters, h is the instantaneous displacement, h_f is the final deformation after the total indenter withdrawn and P is the applied load.

Sneddon theories [25] indicated that the m parameter depends on the indenter geometry. The OP approach suggests 1.5 as the most adequate value for m, using a Berkovich indenter, which corresponds to a revolution paraboloid. However, m values experimentally obtained deviate from the theoretical ones [25,27–30] which indicate that the proposed power law function could possibly inadequate describe the upper portion of the unload curve.

Gong, Miao and Peng (GMP) approach [28–30] uses a power law equation very similar to the one applied by the OP model, but it supposes the indenter geometry being conical, turning the power law to a grade two polynomial approximation, i.e., considering $m = 2$. The GMP model also has the application of a virtual load P_0 in order to consider the residual contact stress which exists along the interface between the plastic hardness impression and the elastic matrix in the material, which is taken by the GMP model as responsible for the variation of the m value [28]. The equation used is displayed as:

$$P = \beta \, (h - h_f)^2 - P_O \tag{3}$$

The main disadvantage of the application of diverse models is the difficulty of agreement among them, leading to different hardness values for the same material. This complicates the behavior understanding, since each approach considers a specific aspect of the contact problem between indenter and sample. The search for relationships among them could facilitate the comprehension of the materials indentation phenomena at low loads, permitting a direct correspondence between the hardness values obtained by each model. The success of this procedure could lead to a unified approach for indentation measurements.

The aim of this work is to measure mechanical properties of bulk materials in accordance with ISO 14,577 Martens model [24,31], the Oliver – Pharr method [25,27] and the approximation developed by Gong, Miao and Peng [28–30] which are typically used on Indentation Hardness Tests (IHT), in order to obtain a relation between the tip correction model and the hardness values as a function of the applied load.

2. Experimental procedure

Commercial aluminum bulk sample was cut from a rod and polished using sandpapers from 100 to 4000 and surface finished with SiC with 250 nm. The silicon p-type (1 0 0) from Temic Semiconductor GmbH, and soda-lime glass (knittel Gläser GmbH) already presented a satisfactory surface polishing.

The IHT measurements were performed using a Fischerscope HV100 equipment (Helmuth-Fischer GmbH, Germany – 2009) equipped with a Berkovich indenter. The load is applied through the action of a solenoid with an accuracy of 0.4 μN and the indenter displacement is measured with a capacitive sensor with a precision of 2 nm in depth.

The bulk samples were submitted to load-unload cycles 3 mN, 5 mN, 10 mN, and 25 mN. The equipment was calibrated according to the ISO 14577 [24], DIN 50 359 [32] and VDI / VDE 2616 [33] standards. One measurement corresponds to an individual cycle which was made with a total time of 120 s, being 60 s for loading e 60 s for unloading, without holding load time. A total number of 10 measurements were made for each sample, resulting in a mean hardness value. The difference between each individual measurement and the mean hardness value were always lower than 5%. The minimum distance between each measurement was of 300 μm avoiding any interference among them. The approaches applied to calculate the hardness values were the OP model and the GMP model, besides Martens model, which is based on the indentation size effect (ISE) [30,33–35] with an indenter tip correction and is determined by ISO 14577 [24]. All the calculation was performed exactly as proposed by the models.

The OP hardness values were calculated according to the model as described on [25,27] using $m = 1.5$ and $m = 2$. The reason to use both values was to assess the indenter response according to both geometries, using the OP model. Basically, 80% of the upper unload curve was adjusted using the Equation (2). After that, the curve was submitted to a linear fit at the peak load. The effective contact depth h_c was calculated by the equation:

$$h_c = h_{\max} - \varepsilon \left(\frac{P_{\max}}{S} \right) \tag{4}$$

where $h_{\max}$ is the maximum displacement, $P_{\max}$ the maximum load applied, S the contact stiffness and ε is equal to 0.75, which corresponds to a Berkovich geometry as determined by Sneddon [26].

The projected area left on the material was calculated by:

$$A = 24.5 \, (h_c + h_d)^2 \tag{5}$$

where h_d corresponds to the indenter tip length correction. This equation was applied in two ways: without h_d correction and estimating the indenter bluntness (h_d) with a size of 100 nm, as recommended by Fisher-Cripps previous work [36].

The GMP approach was processed using the power law fit described on Eq. (3) also with 80% portion of the unload curve and using an $m = 2$. In this case the only indenter response verified was the conical one, since the GMP model considers it more suitable for IHT [28]. The same procedure executed after the power fit for the OP model was made for the GMP approach.

The hardness values were obtained for all models using the equation:

$$H = \frac{P_{\max}}{A} \tag{6}$$

The results are presented in function of the H and S values obtained for each model.

3. Results and discussion

The hardness values obtained according the OP, GMP and Martens models using m = 1.5 and m = 2 *without* h_d *correction* are presenting on Table 1.

The values obtained for the bulk materials are very similar, mostly for the Al sample. This is due to high plasticity of the material, guarantying an adequate contact between the sample and the indenter. However, the values found for Si(1 0 0) are considered high, especially at 3 mN and 5 mN loads. These results indicate the difficulty to achieve an adequate contact between indenter and sample, mainly when the material present high stiffness. The Si (1 0 0) sample presented the higher hardness difference for each model, varying among 29 GPa to 35 GPa approximately at 3 mN. This hardness value decreases significantly when the load is 25 mN, reaching values among 8 GPa and 16 GPa approximately. In a previous work, Guillemot et al. [21] and Beegan et al. [22] are showed the same difference without h_d correction for several hardness models. These results reveal clearly that indenter bluntness should be considered for all cases, even for materials presenting high plasticity. When evaluating surface mechanical properties, such as in oxidized layers or thin films, it is of fundamental importance to understand the implications of using low loads and to employ an appropriate model of tip correction. Rahmound et al. [37] and Puchi-Cabrera et al. [38] compared the use of several IHT models for multilayer coatings demonstrating the importance of these corrections to obtain more realistic hardness values in these complex systems.

The hardness values obtained according the OP, GMP and Martens models using m = 1.5 and m = 2 *considering* h_d *correction* are presenting on Table 2.

The results present good agreement with literature and low deviation even at low loads. Another important feature observed is the minor influence of the m value when the correction of the indenter bluntness is considered. In a recent work, Chicot et al. [39] showed the importance of indenter shape and geometry correction for Berkovich, Vickers, Knoop and spherical indenters. In this work they conclude that the instrumented indentation at a microscopic scale is a valuable tool for determining the elastic modulus and hardness of a material if the calculation of the contact area takes into account the tip defect, that agree with our results.

Chicot et al. [39] used the total compliance term, which corresponds to the inverse of the contact stiffness S (calculated from the slope of the unloading curve at the peak load - P_{max}). In our work the IHT measurements were also performed and analyzed according the hardness models revealing a strong dependence of contact stiffness *S* with the effective contact depth h_c. This relationship shows a linear behavior between S and h_d, as can be seen on Fig. 1.

The analysis of the angular coefficient α obtained for each linear fit indicates an indenter response which is almost equal for the Al and the glass samples displayed on Fig. 1(a) and (b). The Al sample results presents α = 572 mN. μm^{-2} approximately for the OP model using m = 1.5 ($OP_{1.5}$) and the GMP approach, showing the very same linear behavior for both. The OP model with m = 2 ($OP_{2.0}$) and the Martens model presented also very near values for α on

Table 1
Resulting hardness values *without* h_d *correction* obtained according to the OP model using m = 1.5 and 2, GMP approach and Martens model.

$Load_{max}$ [mN]	Samples	Hardness [GPa]			
		OP model		GMP model	Martens model
		m = 1.5	m = 2	m = 2	
03	Al	0.909	0.890	0.936	1.612
	Soda – lime glass	13.134	12.440	11.691	13.641
	Si (1 0 0)	35.141	29.912	34.440	31.011
05	Al	0.667	0.668	0.664	1.362
	Soda – lime glass	7.908	6.926	7.442	11.028
	Si (1 0 0)	21.787	19.104	19.324	22.720
10	Al	0.539	0.541	0.540	1.288
	Soda – lime glass	5.190	4.660	4.992	9.382
	Si (1 0 0)	13.666	12.002	11.440	18.210
25	Al	0.446	0.450	0.444	1.241
	Soda – lime glass	3.666	3.349	3.557	8.703
	Si (1 0 0)	8.694	7.802	7.431	15.780

Table 2
Resulting hardness values obtained according to the OP model using m = 1.5 and 2, GMP approach and Martens model applying h_d correction.

$Load_{max}$ [mN]	Samples	Hardness [GPa]			
		OP model		GMP model	Martens model
		m = 1.5	m = 2	m = 2	
03	Al	1.165	1.169	1.162	1.326
	Soda – lime glass	3.487	3.474	3.508	4.007
	Si (1 0 0)	7.389	7.389	7.476	8.414
05	Al	1.046	1.052	1.040	1.182
	Soda – lime glass	3.309	3.279	3.320	3.801
	Si (1 0 0)	6.656	6.701	6.720	7.581
10	Al	0.986	0.995	0.979	1.128
	Soda – lime glass	3.235	3.201	3.242	3.714
	Si (1 0 0)	6.429	6.548	6.525	7.322
25	Al	0.955	0.972	0.950	1.096
	Soda – lime glass	3.208	3.172	3.211	3.681
	Si (1 0 0)	6.266	6.376	6.346	7.136

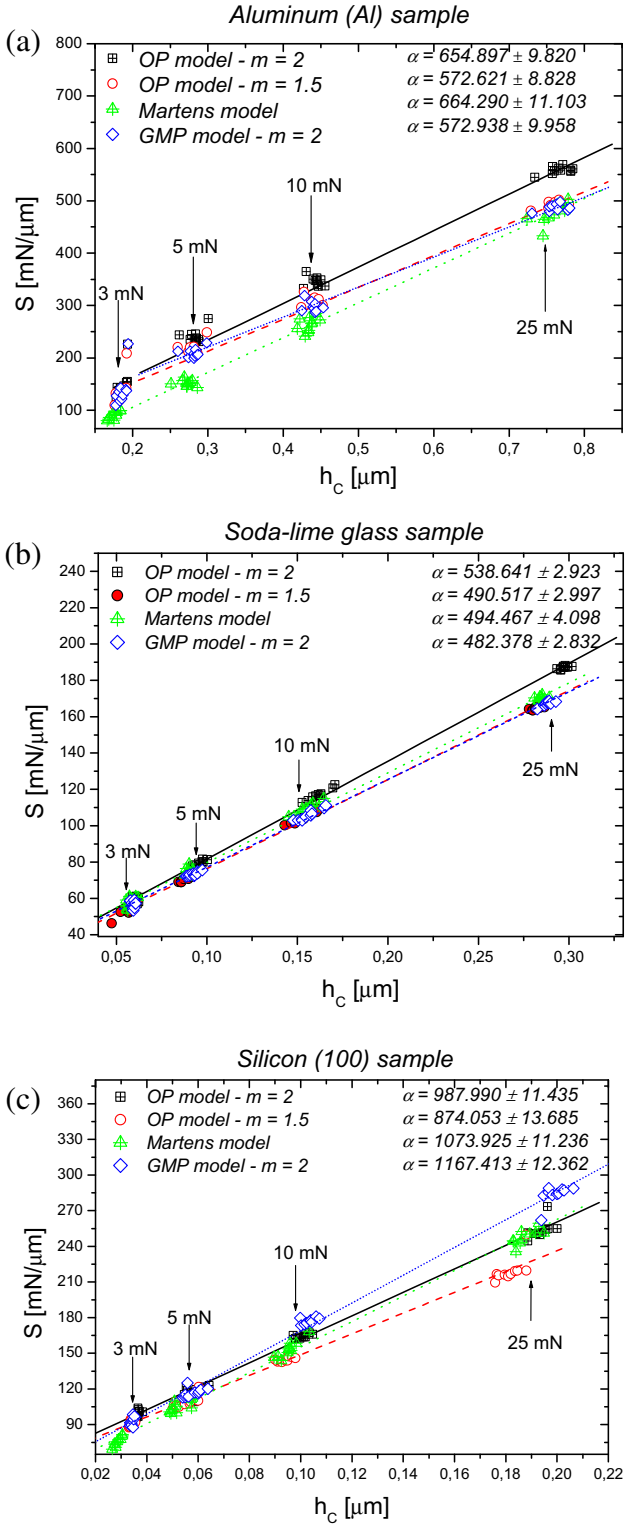

Fig. 1. Linear relation between S and h_c verified for each sample, which corresponds to (a) aluminum, (b) soda-lime glass and (c) silicon (1 0 0).

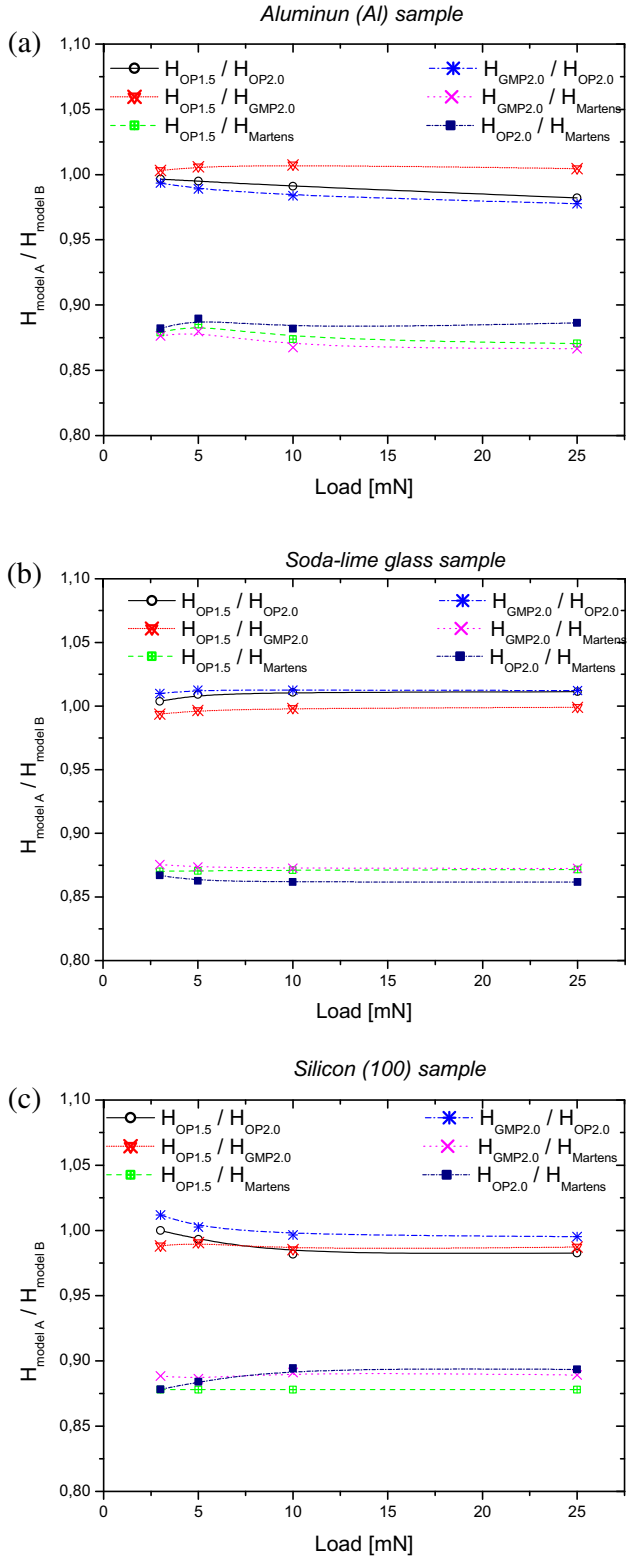

Fig. 2. Hardness ratios according to each applied model and its relationship with the load for the samples, which corresponds to (a) aluminum, (b) soda-lime glass and (c) silicon (1 0 0).

the Al sample. The glass sample presented very near α values, excepting for the $OP_{2.0}$, which showed the same linear behavior for both Al and glass samples, diverging only for Si (1 0 0) sample.

The Si (1 0 0) sample presented a different result, which could be cleared observed for the $OP_{1.5}$ and the GMP linear fits. The difference between the α values for both models is significant and both linear adjust are divergent insofar as the load increases. The Martens model and the $OP_{2.0}$ presented almost the same behavior.

The results show the indenter response is intimately related to the rigidity of the material and the difficulty to produce a

penetration. Evidently, the hardness of a material, as it elastic modulus, and an adequate surface finishing, play an important role on IHT measurements. The results clear state that the indenter bluntness should be monitored from time to time, in order to consider an adequate contact between sample and the indenter. The results also confirm that the indenter shape parameter m lightly affects the measurements, with all influence heavily related to the tip correction.

In order to compare the tree models studied in this work, hardness ratios *using h_d correction* were calculated for all samples and the results are present on Fig. 2. All the hardness ratios involving only $OP_{2.0}$, $OP_{1.5}$ and GMP values are similar, revealing an almost 1.00 constant ratio. When the Martens results are considered, the ratio drops to about 0.87 revealing the influence of the indentation size effect model and tip geometry in the hardness values. It is observed that the h_d correction plays an important role on the measurements and the indenter tip shape could alter significantly the results.

The hardness behavior of the material, the change in OP, GMP and Martens hardness as a function of the indentation displacement, to represent the hardness-load dependence, have been analyzed. Independently on the indenter shape (represented by m), the OP and GMP hardness models considers the projected contact area, whereas the Martens hardness involves the actual contact area between the indenter and the deformed material. The hardness ratios shown in Fig. 2 point to an equivalence between the OP and GMP models that presented similar values of hardness always of the order of 10% lower than the Martens model.

On the other hand, when the tip correction is introduced into the hardness calculation, it is remarkable that the hardness, OP, GMP or Martens, reaches a value approximately constant independent of the applied load and indented depth.

4. Final considerations

The IHT measurements were successful made achieving an elasto–plastic behavior for all materials. The correction of the indenter tip showed a major influence on the results, presenting diverse hardness values when h_d was not considered. The importance of this result state that is necessary to seriously evaluate the indenter bluntness in order to performs adequate nanohardness measurements. The hardness values also indicate that the most significant problem is related to indenter tip shape instead of the form of the load-unload cycle application, the geometry of the indenter and model used.

A clearly dependence between the contact stiffness S and the effective contact depth was observed. A relationship among the hardness values obtained for the samples was verified, revealing the OP model and GMP model are very similar, resulting in hardness values almost equal. Both approaches behavior were also very similar when the indenter geometry was considered as conical ($m = 2$). The use of different m values presented very similar responses mostly for the Al and glass samples, indicating the modification of the original OP model by the GMP approach is of low effectiveness.

Regardless of the model used, the hardness measurements showed behaviors independent of the applied load for all samples measured in this work when the ISE is considered into the hardness calculation.

Acknowledgements

The authors want to thank to the Brazilian Founding Agency CNPq for the financial suport.

References

[1] H. Tateuchi, S. Shiratori, N. Ichihashi, The effect of three-dimensional postural change on shear elastic modulus of the iliotibial band, J. Electromyogr. Kinesiol. 28 (2016) 137–142, https://doi.org/10.1016/j.jelekin.2016.04.006.
[2] T. Lu, J. Wen, S. Qian, H. Cao, C. Ning, X. Pan, X. Jiang, X. Liu, P.K. Chu, Enhanced osteointegration on tantalum-implanted polyetheretherketone surface with bone-like elastic modulus, Biomaterials 51 (2015) 173–183, https://doi.org/10.1016/j.biomaterials.2015.02.018.
[3] J. Liang, K.D. Smith, H. Lu, T.W. Seale, R.Z. Gan, Mechanical properties of the Papio anubis tympanic membrane: change significantly from infancy to adulthood, Hear. Res. 370 (2018) 143–154, https://doi.org/10.1016/j.heares.2018.10.010.
[4] P.-J. Hou, K.-L. Ou, C.-C. Wang, C.-F. Huang, M. Ruslin, E. Sugiatno, T.-S. Yang, H.-H. Chou, Hybrid micro/nanostructural surface offering improved stress distribution and enhanced osseointegration properties of the biomedical titanium implant, J. Mech. Behav. Biomed. Mater. 79 (2018) 173–180, https://doi.org/10.1016/j.jmbbm.2017.11.042.
[5] J. Kim, M.C. Staiculescu, A.J. Cocciolone, H. Yanagisawa, R.P. Mecham, J.E. Wagenseil, Crosslinked elastic fibers are necessary for low energy loss in the ascending aorta, J. Biomech. 61 (2017) 199–207, https://doi.org/10.1016/j.jbiomech.2017.07.011.
[6] V. Goriainov, R. Cook, J.M. Latham, D.G. Dunlop, R.O.C. Oreffo, Bone and metal: An orthopaedic perspective on osseointegration of metals, Acta Biomater. 10 (2014) 4043–4057, https://doi.org/10.1016/j.actbio.2014.06.004.
[7] R. Hübler, A. Cozza, T.L. Marcondes, R.B. Souza, F.F. Fiori, Wear and corrosion protection of 316-L femoral implants by deposition of thin films, Surf. Coat. Technol. 142–144 (2001) 1078–1083, https://doi.org/10.1016/S0257-8972(01)01321-4.
[8] M. Ladinek, A. Niederwanger, R. Lang, An individual fatigue assessment approach considering real notch strains and local hardness applied to welded joints, J. Constr. Steel Res. 148 (2018) 314–325, https://doi.org/10.1016/j.jcsr.2018.06.005.
[9] V.J. Trava-Airoldi, G. Capote, L.F. Bonetti, J. Fernandes, E. Blando, R. Hübler, P.A. Radi, L.V. Santos, E.J. Corat, Deposition of hard and adherent diamond-like carbon films inside steel tubes using a pulsed-DC discharge, J. Nanosci. Nanotechnol. 9 (6) (2009) 3891–3897, https://doi.org/10.1166/jnn.2009.NS85.
[10] G. Strapasson, P.C. Badin, G.V. Soares, G. Machado, C.A. Figueroa, R. Hubler, A.L. Gasparin, I.J.R. Baumvol, C. Aguzzoli, E.K. Tentardini, Structure, composition, and mechanical characterization of dc sputtered TiN-MoS2 nanocomposite thin films, Surf. Coat. Technol. 205 (2011) 3810–3815, https://doi.org/10.1016/j.surfcoat.2011.01.044.
[11] M.M. ElFaham, A.M. Alnozahy, A. Ashmawy, Comparative study of LIBS and mechanically evaluated hardness of graphite/ rubber composites, Mater. Chem. Phys. 207 (2018) 30–35, https://doi.org/10.1016/j.matchemphys.2017.12.036.
[12] W.L. Goh, Y. Zheng, J. Yuan, K.W. Ng, Effects of hardness of steel on ceramic armour module against long rod impact, Int. J. Impact Eng. 109 (2017) 419–426, https://doi.org/10.1016/j.ijimpeng.2017.08.004.
[13] C. Moreau, M. Le Pipec, S. Tence, J. Hemery, J. Rigo, C. Guérin, D. Ruelloux, C. Schneider, P. Le Helleye, A complete methodology for assessing GaN behaviour for military applications, Microelectron. Reliab. 50 (2010) 1587–1592, https://doi.org/10.1016/j.microrel.2010.07.093.
[14] P. Asteriou, G. Tsiambaos, Effect of impact velocity, block mass and hardness on the coefficients of restitution for rockfall analysis, Int. J. Rock Mech. Min. Sci. 106 (2018) 41–50, https://doi.org/10.1016/j.ijrmms.2018.04.001.
[15] P. Małkowski, Ł. Ostrowski, J. Brodny, Analysis of Young's modulus for Carboniferous sedimentary rocks and its relationship with uniaxial compressive strength using different methods of modulus determination, J. Sustainable Min. 17 (2018) 145–157, https://doi.org/10.1016/j.jsm.2018.07.002.
[16] M.F. Doerner, W.D. Nix, A method for interpreting the data from depth-sensing indentation instruments, J. Mater. Res. 1 (4) (1986) 601–609, https://doi.org/10.1557/JMR.1986.0601.
[17] J.L. Loubet, J.M. Georges, G. Meille, Vickers indentation curves of elastoplastic materials; in: Microindentation Techniques in Material Science and Engineering: ASTM Special Technical Publication 889, ISBN 0-8031-0441-3, 1985
[18] W.D. Nix, Elastic and plastic properties of thin films on substrates: nanoindentation techniques, Mater. Sci. Eng., A 234–236 (1997) 37–44, https://doi.org/10.1016/S0921-5093(97)00176-7.
[19] M.F. Doerner, W.D. Nix, M.L. Öveçolu, Elastic interactions of screw dislocations in thin films on substrates, Acta Metall. 35 (1987) 2947–2957, https://doi.org/10.1016/0001-6160(87)90294-X.
[20] X.-Q. Chen, H. Niu, D. Li, Y. Li, Modeling hardness of polycrystalline materials and bulk metallic glasses, Intermetallics 19 (9) (2011) 1275–1281, https://doi.org/10.1016/j.intermet.2011.03.026.
[21] G. Guillemot, A. Iost, D. Chicot, Comments on the paper "Modification of composite hardness models to incorporate indentation size effects in thin films", D. Beegan, S. Chowdhury and M.T. Laugier, Thin Solid Films 516 (2008), 3813–3817, Thin Solid Films, 518 (8) (2010) 2097–2101. http://dx.doi.org/10.1016/j.tsf.2009.07.178.
[22] D. Beegan, S. Chowdhury, M.T. Laugier, Modification of composite hardness models to incorporate indentation size effects in thin films, Thin Solid Films 516 (12) (2008) 3813–3817, https://doi.org/10.1016/j.tsf.2007.06.140.

[23] A. Iost, G. Guillemot, Y. Rudermann, M. Bigerelle, A comparison of models for predicting the true hardness of thin films, Thin Solid Films 524 (2012) 229–237, https://doi.org/10.1016/j.tsf.2012.10.017.
[24] ISO, 14577, Metallic Materials – Instrumented indentation test for hardness and materials parameters. Part 1, Test method (2002).
[25] W.C. Oliver, G.M. Pharr, An improved technique for determining hardness and elastic modulus using load and displacement sensing indentation experiments, Mater. Res. Soc. 7 (1992) 1564–1583, https://doi.org/10.1557/JMR.1992.1564.
[26] I.N. Sneddon, The relation between load and penetration in the axisymmetric Boussinesq problem for a punch of arbitrary profile, Int. J. Eng. Sci. 3 (1965) 47–57, https://doi.org/10.1016/0020-7225(65)90019-4.
[27] G.M. Pharr, W.C. Oliver, F.R. Brotzen, On the generality of the relationship among the contact stiffness, contact area and elastic modulus during indentation, J. Mater. Res. 7 (1992) 613–617, https://doi.org/10.1557/JMR.1992.1564.
[28] J. Gong, H. Miao, Z. Peng, Analysis of the nanoindentation data measured with a Berkovich Indenter for brittle materials: effect of the residual contact stress, Acta Mater. 52 (2004) 785–793, https://doi.org/10.1016/j.actamat.2003.10.013.
[29] J. Gong, H. Miao, Z. Peng, A new function for the description of the nanoindentation unloading data, Scr. Mater. 49 (1) (2003) 93–97, https://doi.org/10.1016/S1359-6462(03)00174-X.
[30] J. Gong, H. Miao, Z. Peng, On the contact area for nanoindentation tests with Berkovich indenter: case study on soda-lime glass, Mater. Lett. 58 (7–8) (2004) 1349–1353, https://doi.org/10.1016/j.matlet.2003.09.026.
[31] A.C. Fischer-Cripps, A review of analysis methods for sub-micron indentation testing, Vacuum 58 (2000) 569–585, https://doi.org/10.1016/S0042-207X(00)00377-8.
[32] DIN, 50 359; Testing of metallic materials, Universal hardness testing (1998).
[33] VDI/VDE 2616; Hardness testing of metallic materials, 1998.
[34] V. Marx, H. Balke, A critical investigation of the unloading behavior of sharp indentation, Acta Mater. 45 (1997) 3791–3800, https://doi.org/10.1016/S1359-6454(97)00031-1.
[35] J. Woirgard, J.-C. Dargenton, C. Tromas, V. Audurier, A new technology for nanohardness measurements: principle and applications, Surf. Coat. Technol. 100–101 (1998) 103–109, https://doi.org/10.1016/S0257-8972(97)00597-5.
[36] A.C. Fischer-Cripps, Critical review of analysis and interpretation of nanoindentation test data, Surf. Coat. Technol. 200 (2006) 4153–4165, https://doi.org/10.1016/j.surfcoat.2005.03.018.
[37] K. Rahmoun, A. Iost, V. Keryvin, G. Guillemot, N.E. Chabane Sari, A multilayer model for describing hardness variations of aged porous silicon low-dielectric-constant thin films, Thin Solid Films (518(1), 2009,) 213–221, https://doi.org/10.1016/j.tsf.2009.07.040.
[38] E.S. Puchi-Cabrera, M.H. Staia, A. Iost, Modeling the composite hardness of multilayer coated systems, Thin Solid Films 578 (2) (2015) 53–62, https://doi.org/10.1016/j.tsf.2015.01.070.
[39] D. Chicot, P. Baets, M.H. Staia, E.S. Puchi-Cabrera, G. Louis, Y.P. Delgado, J. Vleugels, Influence of tip defect and indenter shape on the mechanical properties determination by indentation of a TiB2–60%B4C ceramic composite, Int. J. Refract. Met. Hard. Mater. 38 (2013) 102–110, https://doi.org/10.1016/j.ijrmhm.2013.01.006.